Dyes and Pigments 197 (2022) 109884

Contents lists available at ScienceDirect

Dyes and Pigments

journal homepage: www.elsevier.com/locate/dyepig

Near-infrared absorbing hydrogen-bonded dithioketopyrrolopyrrole (DTPP) n-type semiconductors

Matous Kratochvil [a,1], Martin Ciganek [a,1], Cigdem Yumusak [a,b], Hathaichanok Seelajaroen [b], Ivana Cisarova [c], Jan Fabry [d], Martin Vala [a], Stanislav Lunak [a], Martin Weiter [a], Niyazi Serdar Sariciftci [b], Jozef Krajcovic [a,*]

[a] Brno University of Technology, Faculty of Chemistry, Materials Research Centre, Purkyňova 118, 612 00, Brno, Czech Republic
[b] Linz Institute for Organic Solar Cells (LIOS), Physical Chemistry, Johannes Kepler University Linz, Altenbergerstraße 69, 4040, Linz, Austria
[c] Department of Inorganic Chemistry, Faculty of Science, Charles University, Hlavova 2030, CZ, 128 00, Prague, Czech Republic
[d] Institute of Physics of the Czech Academy of Sciences, Na Slovance 1999/2, 182 21, Prague, Czech Republic

ARTICLE INFO

Keywords:
Organic photovoltaics
Hydrogen-bonded pigments
Dithioketopyrrolopyrrole
Diketopyrrolopyrrole
n-type semiconductors

ABSTRACT

Optical and semiconducting properties of vacuum-deposited thin films of four hydrogen-bonded pigments were studied. Well-known 1,4-diketo-3,6-diphenyl-pyrrolo-[3,4-*c*]-pyrrole (Ph-DPP) and 1,4-diketo-3,6-(thiophen-2-yl)-pyrrolo-[3,4-*c*]-pyrrole (Th-DPP) were transformed to their 1,4-dithioketo heteroanalogues (Ph-DTPP and Th-DTPP) using Lawesson's reagent. X-ray single crystal structure determination confirmed the presence of CS-HN hydrogen bonds and a similar stack formation in both DTPPs, leading to relatively high decomposition temperatures, about 350 °C. According to density functional theory (DFT) calculations, thionation left HOMO (π-type) level almost unchanged, considerably destabilized non-bonding orbital (n-orbital) localized on thioketo group, and significantly decreased LUMO (π*-type) energy. Evolution of HOMO and LUMO energies was confirmed by cyclic voltammetry, establishing LUMO energy at −4.5 eV for both DTPPs, while a signature of high-lying n-orbital was detected through nπ* transition in the far-red/near-infrared area of absorption spectra, interpreted with help of time dependent DFT calculations on monomer and stacked dimer geometry. The lowest optical band-gap among the pigments under study was found to be 1.4 eV for Ph-DTPP thin film. Field effect mobilities, determined on a bottom-gate top-contact transistor, show DPPs as p-type and DTPPs as n-type semiconductors. The highest electron mobility $\mu_e = 0.018$ cm^2 V^{-1} s^{-1} was obtained for Ph-DTPP film in the device with aluminium source and drain electrodes.

1. Introduction

Organic photovoltaics (OPV) based on all-small-molecules, i.e. small (non-polymer) both electron-donor and non-fullerene electron-acceptor (NFA), belongs to the hot research topics in material science [1]. Consequently, the search for the NFA molecules with NIR absorption (narrow band-gap < 1.5 eV) and high electron mobility is of primary interest [2]. n-Type organic semiconductors (OSC) generally suffer from oxidation of their reduced state by traces of oxygen and water [3]. Therefore, LUMO energies under −4.0 eV are required for their ambient performance [4]. The application of hydrogen-bonded (H-bonded) organic pigments (OP) as OSCs is considered as a general strategy to improve overall operational stability of electronic devices [5]. The disadvantage of OPs is their insolubility, i.e. inability to be processed from solution, but the progress in vacuum-processed OPV gives them a chance to be used as the components of solar cells [6].

Diketopyrrolopyrroles (DPP), like 1,4-diketo-3,6-diphenyl-pyrrolo-[3,4-*c*]-pyrrole (**Ph-DPP** in Fig. 1, P.R. 255 according to Color Index), were originally developed as high-performance organic pigments [7]. In contrast to some pyridyl heteroanalogues [8], all on-phenyl substituted **Ph-DPP** derivatives show exclusively strong multiple intermolecular H-bonding of CO–HN type, while slight deviations from planarity and overall packing, including π-stacking pattern, is substituent-dependent [9]. On the contrary to widely reported soluble *N*-alkylated derivatives [10], in which H-bonding is disabled, X-ray structures of DPP derivatives with five-membered rings (like **Th-DPP** in Fig. 1), instead of

* Corresponding author.
E-mail address: krajcovic@fch.vut.cz (J. Krajcovic).
[1] These authors contributed equally.

https://doi.org/10.1016/j.dyepig.2021.109884
Received 22 July 2021; Received in revised form 8 October 2021; Accepted 9 October 2021
Available online 13 October 2021

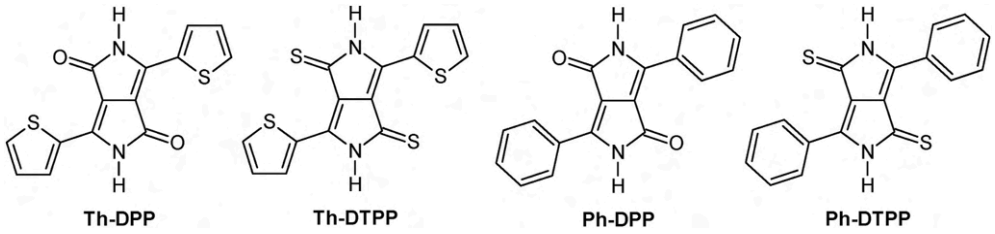

Fig. 1. DPP and DTPP materials under study.

3,6-phenyls, were not reported. Thionation of **Ph-DPP** with Lawesson's reagent or P_4S_{10} leads to **Ph-DTPP** [11], for which three crystal modifications were described [12]. **Ph-DTPP** molecules in all three polymorphs are H-bonded (CS–HN) and show various phenyl twists from planarity (6°–30°). In difference to its soluble *N,N′*-dioctyl derivative [13], **Th-DTPP** pigment was reported only as an intermediate for *S*-alkylated diazapentalenes [14], without any physical properties.

According to cyclic voltammetry (CV), carried out on soluble DPP and DTPP monomers [13,15], polymers [16] and iso**Th-DPP** regioisomers [17], the effect of thionation on the energy of frontier π-orbitals is qualitatively always the same: LUMO level is stabilized and HOMO is destabilized. Consequently, the absorption spectra in solution show always red shift upon thionation. Thionation of only one keto group in DPP leads to a complete quenching of fluorescence in solution [15,16]. Identical effect was observed in thionated perylene diimides [18] and oxadiazoles [19] and explained by El Sayed rules [20], i.e. by promoting of intersystem crossing (ISC), due to high-lying singlet nπ* state, localized on the thioketo group.

As observed in organic field-effect transistors (OFET), *N,N′*-dialkylated derivatives of **Th-DPP** are typical p-type semiconductors (hole mobilities ~10^{-2}–10^{-1} cm^2/Vs) [10i, 21], although some opposing examples can be found [10j]. On the other hand, some *N,N′*-dialkylated DPP polymers, based on **Th-DPP** core [3b] show often n-type unipolar or ambipolar behaviour [3b]. Semiconducting properties of H-bonded DPPs generally use two ways to prepare active channels in OFETs: vacuum deposition of H-bonded pigment or thermal decomposition of solution-processable latent pigments [22]. The first method was used in an investigation of **Ph-DPP** pigment and its halogenated derivatives, showing ambipolar carrier mobilities (hole and electron mobilities ~0.01–0.06 cm^2/Vs) [9c]. The second method enabled to find a dramatic rise of hole mobility (increase up to 0.26 cm^2/Vs), when going from latent to H-bonded **Th-DPP** [23]. The knowledge about effect of thionation on semiconducting characteristics of DPPs is limited. An increase of hole mobility of DPP polymer with *N,N′*-dialkylated **Th-DPP** core was recently reported [24] and a switch from unipolar p-type to ambipolar behaviour was observed for a polymer with *N,N′*-diarylated iso**Th-DPP** core [17b]. There are no reports on DTPP small molecule OSCs either H-bonded, or soluble.

The above mentioned state-of-the-art motivated us to study the optical and semiconducting properties of two representative DTPP pigments. More precisely, we were interested, whether these compounds are able to form stable, low band-gap, low LUMO n-type semiconductors with a potential in organic optoelectronics. Due to the insufficient solubility most of the physical experiments had to be carried out on vacuum-deposited thin films of DTPPs (and starting DPPs for comparison).

2. Experimental

2.1. Materials

2-Thiophenecarbonitrile (99%), benzonitrile (anhydrous, ≥99%), sodium, iron(III) chloride (>97%, anhydrous), *tert*-amyl alcohol (≥99%), *N,N*-dimethylformamide (DMF) (99.8%, anhydrous), Lawesson's reagent (97%), chlorobenzene (anhydrous, 99.8%) and dimethyl sulfoxide-d_6 (99.9 atom % D) were purchased from Sigma-Aldrich (now Merck) and were used as received. Diisopropyl succinate (98%) was purchased from Synthesia, Inc. and was used as received. Acetic acid (99%), isopropyl alcohol (p.a.) and methanol (p.a.) were purchased from PENTA Ltd. and were used as received. Dimethyl sulfoxide (DMSO) (p. a.) was purchased from VWR and was used as received.

2.2. Synthesis

Th-DPP and **Ph-DPP** were synthesized, as previously, from corresponding nitrile and succinate [25]. Thioketo analogues of DPPs (**Th-DTPP** and **Ph-DTPP**) were prepared *via* thionation of the DPP derivative using Lawesson's reagent (LR) in chlorobenzene as a solvent and at reflux for several hours [11]. Detailed synthesis and characterizations of all studied compounds (**Th-DPP**, **Ph-DPP**, **Th-DTPP** and **Ph-DTPP**) are elaborated in Electronic Supplementary information (ESI).

2.3. Nuclear magnetic resonance (NMR) characterization

^{1}H NMR spectra were recorded on an FT-NMR spectrometer Bruker AVANCE™ III 300 MHz or 500 MHz. ^{13}C NMR spectra were recorded on an FT-NMR spectrometer Bruker AVANCE™ III 500 MHz. The solvent used was DMSO-d_6. Chemical shifts (δ) are given in parts per million (ppm) relative to tetramethylsilane (TMS) as an internal reference.

2.4. Elemental analysis (EA)

Elemental analysis was measured using an elemental analyser Thermo Scientific™ FLASH 2000 CHNS using sulphanilamide as a standard.

2.5. Thermogravimetric analysis (TGA)

Thermogravimetry (TG) was conducted on a TA Instruments Q5000IR (New Castle, Delaware, USA) in order to analyse the thermal stability of the derivatives and changes in mass before degradation. The samples were placed on the Pt crucible sample holder and heated at 10 °C/min from room temperature to 1000 °C under a stream of nitrogen (ultra-high purity) flow rate 40 mL/min. The TG records (dependence of mass on temperature) were evaluated using TRIOS and Universal analysis software provided by TA Instruments. The TG records were derived, and onsets of the derivatives were determined. The TG records are elaborated in ESI.

2.6. Ultraviolet–visible (UV–Vis) absorption and photoluminescence (PL)

Optical characteristic of the title compounds were studied on their dilute (10–100 μM) solutions in both DMF and DMSO and on thin films (100 ± 5 nm) prepared by physical vapor deposition on clean glass substrates. UV–Vis spectroscopy measurements were carried out using Perkin Elmer Lambda 1050 UV–Vis–NIR spectrophotometer. PL measurements of liquid samples were carried out using PhotoMed PTI fluorimeter, while thin film samples were excited by diode laser and photoluminescence was captured using Shamrock SR-303i-A monochromator equipped with Andor CCD camera (to shield the detector

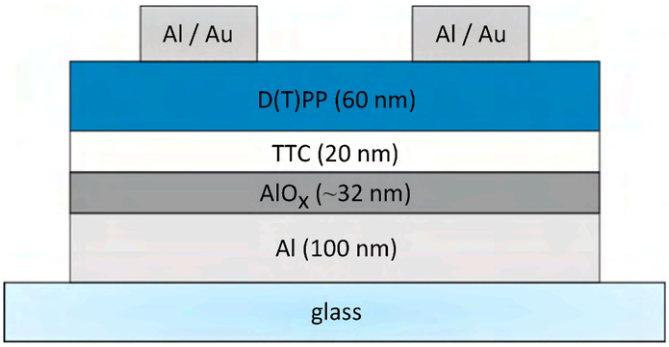

Fig. 2. Device architecture of the fabricated OFETs.

from exciting light, 515 nm or 637 nm long-pass filters were used).

2.7. Vacuum-deposited organic field-effect transistor (OFET) fabrication

The OFETs were fabricated in a staggered bottom-gate, top-contact device configuration (Fig. 2). Glass substrates were sequentially cleaned by the alkaline detergent (Hellmanex), deionized water, acetone and isopropanol in an ultrasonic bath for 15 min each. Aluminium gate electrode (100 nm, rate 1–5 nm/s) was evaporated through shadow mask. Afterwards, 32 nm of anodized amorphous aluminium oxide (AlOx) was grown by using the potentiostatic method [26] on the defined part of the aluminium electrode. The AlO_x layer was subsequently passivated [27] by 20 nm of tetratetracontane (TTC, $CH_3(CH_2)_{42}CH_3$) to create an inorganic/organic composite gate dielectric with a capacitance of 20 nF cm^{-2}. Next, 60 nm of the studied semiconductor material was evaporated ($1{\cdot}10^{-6}$ mbar; rate 0,1-0,3 A s^{-1}). To complete the device, gold or aluminium source and drain electrodes were evaporated using shadow mask (thickness: 80 nm) with the resulting channel of length L = 60 μm and width W = 2 mm.

2.8. Electrochemical measurements

In order to determine the highest occupied molecular orbital (HOMO) and the lowest unoccupied molecular orbital (LUMO) energy levels of all compounds, we conducted the electrochemical measurements using a Jaissle Potentiostat-Galvanostat IMP 83 (Jaissle Elektronik GmbH, Waiblingen, Germany). Cyclic voltammetry (CV) was performed in three-electrode electrochemical system. The set-up consisted of an indium tin oxide (ITO) coated glass slide deposited with respective compound as a working electrode, an Ag/AgCl quasi-reference electrode (QRE) and a Pt plate counter electrode. Electrolyte solution of anhydrous acetonitrile contained 0.1 M tetrabutylammoniumhexafluorophosphate ($TBAPF_6$). Cyclic voltammograms were recorded by scanning potential from 0 to 2.0 or −2.0 V vs Ag/AgCl QRE for the determination of HOMO or LUMO energy level (E_{HOMO} or E_{LUMO}), respectively, with the scanning rate of 25 mV s^{-1}. The potentials were calibrated externally against ferrocene/ferrocenium redox couple of 0.69 V vs. normal hydrogen electrode (NHE) in acetonitrile solution [28]. The energy levels were calculated using following formula from

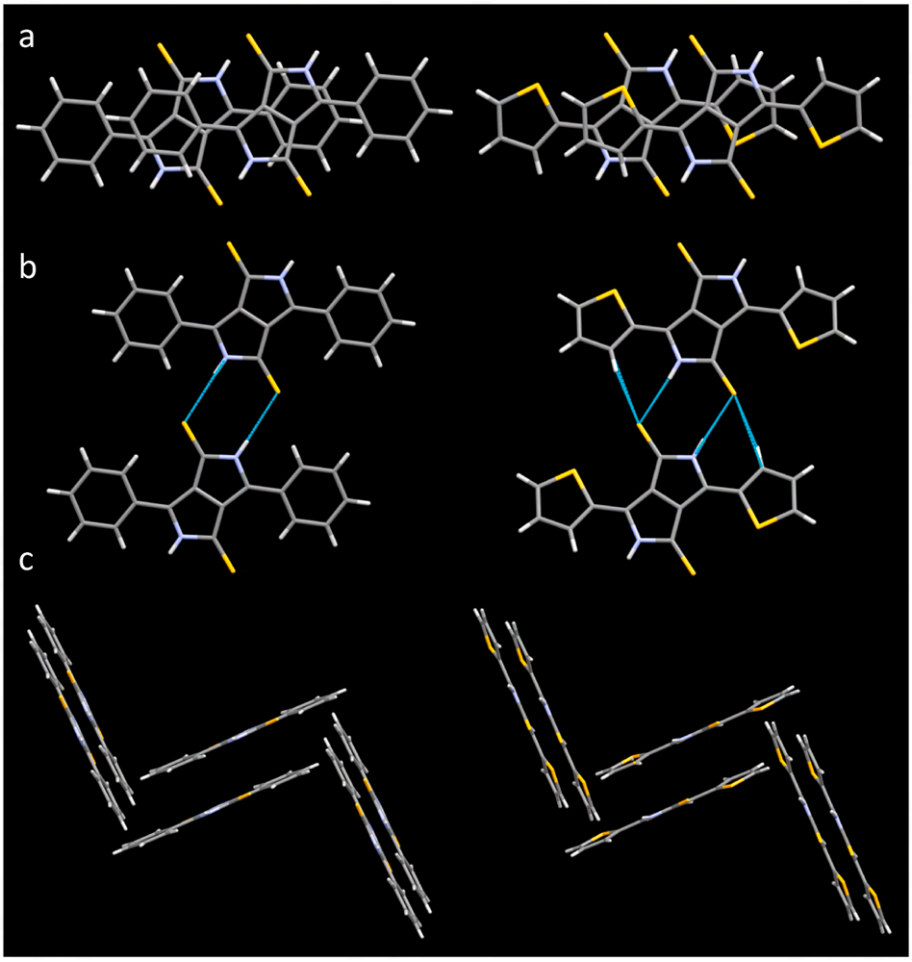

Fig. 3. Crystal packing for **Ph-DTPP** (left) and **Th-DTPP** (right). a) stacked dimer for **Ph-DTPP** and **Th-DTPP** (Table S2); b) H-bonded dimer extracted from crystal structure; c) herringbone packing.

onset potentials [29]:

$$E_{HOMO} = -(4.75\ eV + E_{ox,\ onset}\ vs\ NHE)$$

$$E_{LUMO} = -(4.75\ eV + E_{red,\ onset}\ vs\ NHE)$$

2.9. X-ray single crystal structure determination

XRD data of **Th-** and **Ph-DTPP** were collected at 120 K by the φ and ω scans technique on a Bruker D8 VENTURE Kappa Duo PHOTON 100 CMOS diffractometer with Cu *Kα* radiation, equipped with an Helios Cu multilayer optic monochromator. The approximate structural model for each of the title structure was found by Superflip [30]. The refinement was carried out by *JANA*2006 [31]. In both cases, the aryl hydrogen atoms were attached to the carbon carriers and constrained by the constraints C_{aryl}—H_{aryl} = 0.95 Å and $U_{iso}(H_{aryl})$ = 1.2 $U_{eq}(H_{aryl})$. The positional parameters of the secondary amine hydrogen were refined freely while U_{iso}(H1n1) = 1.2 U_{eq}(N1). Information about the crystal data, data collection and the refinement, solving a positional disorder in **Th-DTPP** crystal and twinning in **Ph-DTPP** crystal, using PLATON software [32], is given in ESI. The structures of **Th-DTPP** and **Ph-DTPP** were deposited with the Cambridge Crystallographic Data Centre (CCDC) under the numbers CCDC-2104737 and CCDC-2104740, respectively.

2.10. Theoretical modelling

All geometries were computed by density functional theory (DFT) using ωB97X-D xc functionals and with 6–31G(d,p) basis set. In few cases also B3LYP with 6-311G(d,p) basis set was used. All optimization were carried out in vacuum. Optimized geometries of monomers and dimers were checked by vibrational analysis. The resulting geometries of the dimers were characterized by plane-to-plane (PP) and centre-to-centre (CC) distances between DPP rings. Excitation energies were calculated by time dependent (TD) DFT on either B3LYP or CAM-B3LYP/6-311+G(2d,p) level, either in vacuum or in DMSO, modelled with polarized continuum (PCM). All calculations were carried out with Gaussian 09 software [33].

3. Results and discussion

3.1. Synthesis and characterization

All four pigments were prepared by known procedures. They show acceptable chemical purity according to $^{1}H/^{13}C$ NMR and EA. No special purification procedures were carried out before measuring optical and electrical properties. All compounds were soluble only in DMSO and DMF to the concentrations necessary for spectral measurements in solution. On the other hand, the concentrations required for CV in solution could not be achieved. Both DTPP compounds show high thermal decomposition temperatures according to TGA (347 °C and 350 °C for **Ph-DTPP** and **Th-DTPP**, respectively), falling into range found for planar, stacked and H-bonded DPPs [25a]. Consequently, no significant degradation was observed during vacuum deposition of thin films. The crystals suitable for XRD were obtained by a sublimation of the powders.

3.2. X-ray single-crystal structures

The crystal structures of **Th-DTPP** and **Ph-DTPP** have similar features. They both crystallize in the same space group type ($P2_1/n$) with two molecules in the unit cell (Z = 2). Both title molecules possess the symmetry $\bar{1}$ since they are situated in the special position (the Wyckoff position 2*a*).

The main cohesion forces between the molecules can be inferred from the arrangement of the molecules in the structure. These are van der Waals forces between the molecules (see ESI), π-ring electron⋯π-ring

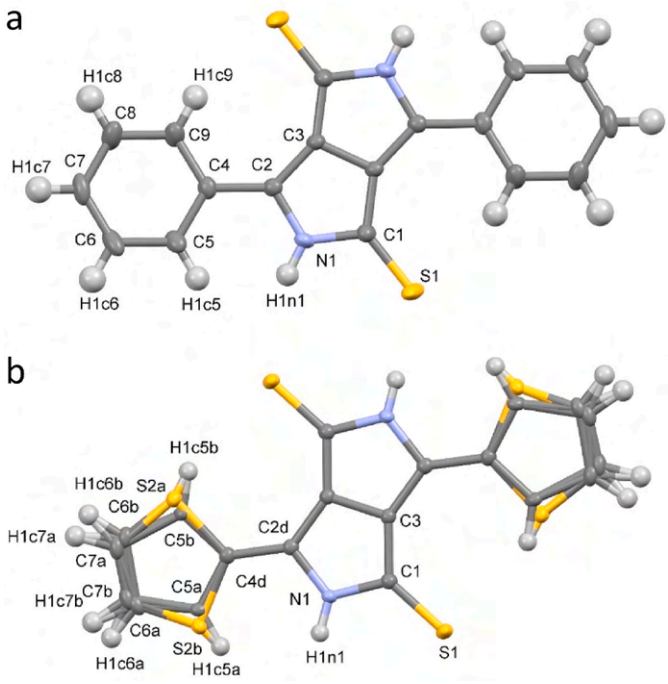

Fig. 4. Molecular structures of a) **Ph-DTPP** and b) **Th-DTPP**. Displacement ellipsoids are shown at the 50% probability level. C, N, S and H atoms are shown as dark grey, blue, yellow ellipsoids and as tiny light-grey spheres, respectively [35].

electron interactions (Table S2), C–H … π-ring electron interactions (Tables S3a and S3b) and the intramolecular hydrogen bonds N–H⋯S1 and C–H⋯S1 (Tables S4a and S4b). On the other hand, **Th-DTPP** is positionally disordered in contrast to the molecule of **Ph-DTPP**. Thus, the molecules in both structures form columns (Fig. 3a) while the molecules in the adjacent columns are interconnected by the hydrogen bonds (Fig. 3b). The crystal packing is herringbone both for **Ph-DTPP** and **Th-DTPP** (Fig. 3c).

The molecule of **Ph-DTPP** is nearly planar (Fig. 4a), with a phenyl twist angle equal to 4.65(9)°. Its crystal structure corresponds to the previously determined polymorph **Ph-DTPP** [34a]; the refcode SIFLOI01; the Cambridge Structural Database [34b]. The title structure is, however, twinned (for the twinning matrix, see ESI) as well as positionally disordered (Fig. 4a). There are known other two polymorphs: one with the refcode SIFLOI [34a] and the other with the refcode SIFLOI02 [34c]. The molecule in the title polymorph is the least deviated one from planarity among the structures obtained for three polymorphs (SIFLOI, SIFLOI01 and SIFLOI02) and two solvates (KOYPET and KOYPIX) [12], see ESI (Table S5). In SIFLOI02 the angles equal to 29.3(2)° and 34.2(2)°.

As it was given above, **Th-DTPP** is positionally disordered (Fig. 4b), containing molecules with thiophenes in *s-trans* (88.9(2) %) and *s-cis* (11.1(2) %) arrangements with respect to the DPP core (see ESI, Scheme S1). A similar disorder was also observed in some *N*-alkylated **Th-DPP** derivatives [10j]. The preference of *s-trans* conformation was described for *N*-acylated **Th-DPP** [10c], but generally, *s-cis* arrangement is more common in **Th-DPP** derivatives [10]. Twist angles in **Th-DTPP** are 6.2(2)° – 8.4(1)°, i.e. a bit larger than in **Ph-DTPP**. The stacking pattern of **Th-DTPP** is quite similar to that observed for **Th-DPP** derivatives *N*-alkylated with linear alkyls, like *n*-hexyl (Fig. 5a), with stacked molecules shifted along long molecular axis. This differs from the pattern observed for the derivatives with *β*-branched alkyls, like isopentyl (Fig. 5b), with a shift along the short axis [10c].

N-alkylated derivatives of **Th-DTPP** show flatter minima of non-planar *s-cis* and *s-trans* conformers and lower barrier of their

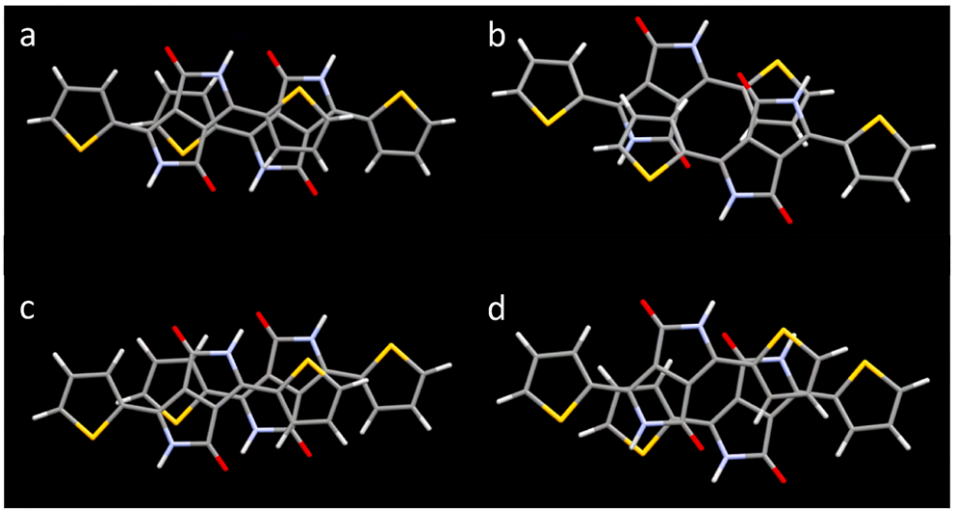

Fig. 5. Stack geometries of **Th-DPP** derivatives. Experimental geometries (up), extracted from files a) BIBDIB01 (C6 substituted by H, PP = 3.408 Å, CC = 5.357 Å, left) and b) UBESAY01 (C5 substituted by H, PP = 3.548 Å, CC = 5.632 Å, left). Corresponding reoptimized geometries (down) on ωB97X-D/6-311G(d,p) level, giving c) PP = 3.237 Å, CC = 4.694 Å, left, and d) PP = 3.243 Å, CC = 4.658 Å, right, respectively.

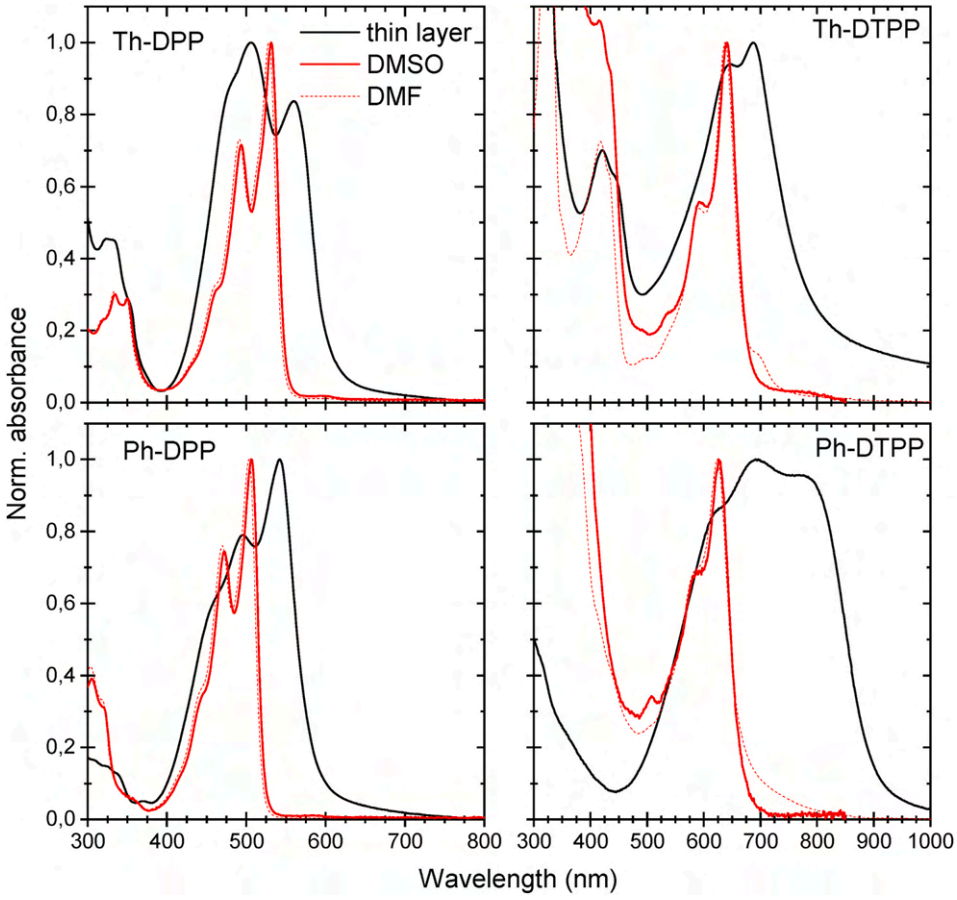

Fig. 6. Absorption spectra in DMSO, DMF and TL.

isomerization [13]. Therefore, the torsional flexibility of DTPPs, manifested by a wide range of twist angles in **Ph-DTPP** polymorphs/solvates and *cis/trans* disorder in **Th-DTPP**, is not so surprising and one can expect a significant effect of intermolecular interactions on molecular geometry. If **Ph-DPP** monomer is optimized on ωB97X-D/6-311G(d,p) level, it gives planar geometry, while **Ph-DTPP** forms centrosymmetrical structure with phenyls twisted by 26°. If the same optimization is carried out for a stacked trimer, with the stacking pattern as on Fig. 3, the central molecule remains centrosymmetrical, but the torsion decreases to 13°. Thus, the difference in twist angles in SIFLOI01 (very similar to the one, presented here) and SIFLOI02 modifications relates to the presence and tightness of stacking interaction. If centrosymmetrical **Th-DTPP** monomers are optimized, *s-cis* conformation is significantly favored with respect to *s-trans* (4.05 kcal mol^{-1}). If one compares the

Table 1
Absorption maxima of studied molecules in thin layer, DMSO and DMF solutions [nm]. A position of long-wavelength local maximum (0-0) in TL absorption of **Th-DPP** is added.

Compound	thin layer	DMSO	DMF
Th-DPP	506; 560	531	528
Th-DTPP	687	641	638
Ph-DPP	542	506	503
Ph-DTPP	696	626	624

energy of optimized stacked dimers, with a pattern as on Fig. 3, the dimer composed only from *s-cis* monomers is considerably more stable than the one, composed from *s-trans* monomers (8.50 kcal mol^{-1}), i.e. the stacking interaction has almost no effect on the preferences between the conformers, as the energy difference between the dimers is about twice higher than for the monomers. On the other hand, if H-bonded dimers are computed, according to the arrangement on Fig. 3, the energy of the one composed of *s-cis* monomers is only 5.47 kcal mol^{-1} lower than for the dimer of *s-trans* monomer, i.e. H-bonding relatively stabilizes *s-trans* conformation. We ascribe this effect to the presence of an additional H-bond (C**S**-H**C** 3.580 Å exp., 3.681 Å theor.) exclusively present in the *s-trans* conformation. As the *s-cis* conformation is also favored for **Th-DPP** and as such an additional H-bonding as in **Th-DTPP** cannot exist, the dominance of *s-cis* arrangement in still unknown packing of **Th-DPP** can be expected. Furthermore, *s-cis* conformation of **Th-DTPP** should be preferred in solution, where stabilizing H-bonding is also missing. The stacking pattern of both DPPs will be discussed together with thin layer (TL) absorption spectra.

3.3. Optical properties

The absorption spectra were measured in DMSO, DMF and on a TL (Fig. 6 and Table 1). The spectra in solution always show three vibronic progressions with an absolute maximum relating to 0-0. Small long-wavelength shoulders are observed for both DTPPs in DMSO. Mutual shifts of the spectral maxima are quite clear and expected: DTPPs are dramatically red shifted (over 100 nm) with respect to DPPs and the replacing of phenyls with thiophenes causes moderate bathochromic shift (25 nm for DPPs and 15 nm for DTPP pair). The spectra in TL remain sharp for both DPPs, but the intensity of progression is considerably redistributed towards higher $R_{ABS} = I_{01}/I_{00}$. 0-0 bands in TL show a similar bathochromic shift with respect to those in solution. Such an evolution is typical for red shifted H-aggregates with small (**Ph-DPP**) and strong (**Th-DPP**) excitonic coupling [36]. The spectra of DTPPs in TL are more complicated. They are broader with less resolved progression. Their absolute maxima show the similar red shifts with respect to those in solution, but an additional absorption appears in long-wavelength region, manifested either by a long unresolved tail (**Th-DTPP**), or as a local maximum (**Ph-DTPP**), as found also previously [12a]. As usual [25a], both DPPs show strong fluorescence in solution (Fig. S12), while for DTPPs this fluorescence is completely quenched. All four pigments show very weak (PLQY < 0.01) solid solid-state fluorescence (Fig. S13).

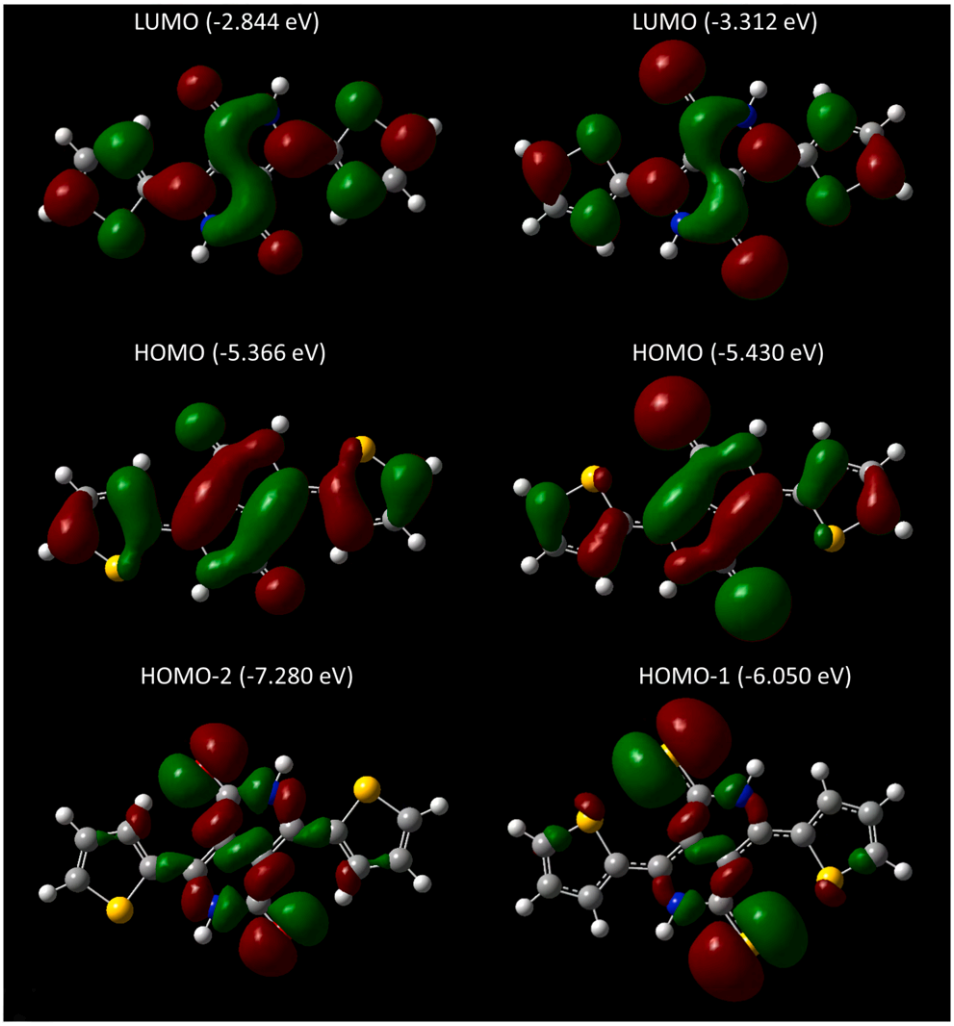

Fig. 7. Kohn-Sham orbitals of **Th-DPP** (*s-cis*, left) and **Th-DTPP** (*s-trans*, right), computed on B3LYP/6-311G(d,p) level in vacuum [37]. Isovalue 0.02 was used.

Table 2
PCM TD DFT calculation of excitation energies (E_{exc}), oscillator strengths (f_{osc}) and transition composition in configurational interaction (CI) of monomers in DMSO, computed on B3LYP/6-311+G(2d,p) level at ωB97X-D/6-31G(d,p) monomer geometry. More planar structure of **Ph-DTPP** was obtained by an optimization of centrosymmetrical stacked trimer and extracting its central monomer. Experimental values E_{abs}, obtained from absorption, are shown for comparison. H = HOMO, L = LUMO.

Compound	Conformer	Twist angle[^{0}]	Transition type	E_{exc} [eV]	f_{osc}	Major configuration in CI [%]	E_{abs} [eV]
Ph-DPP		0	ππ*	2.580	0.618	H→L	2.451
Th-DPP	*s-cis*	0	ππ*	2.444	0.692	H→L	2.235
Ph-DTPP		5	ππ*	2.128	0.369	H→L	1.981
			nπ*	2.039	0.001	H-1→L	
		26	ππ*	2.182	0.288	H→L(61)+ H-1→L(36)	
			nπ*	2.002	0.063	H→L(-36)+ H-1→L(60)	
Th-DTPP	*s-cis*	0	ππ*	2.086	0.412	H→L	1.934
			nπ*	2.131	0.000	H-1→L	
	s-trans	175	ππ*	2.079	0.209	H→L(-46)+ H-1→L(54)	
			nπ*	2.125	0.175	H→L(54)+ H-1→L(46)	

Thionation affects the electronic structure of the molecules (Fig. 7): lets HOMO (π-type, a_g symmetry) almost untouched, significantly stabilizes LUMO (π*-type, a_u symmetry) and dramatically destabilizes thioketo localized n-orbital (HOMO-1, a_g symmetry), as compared to the keto localized one (HOMO-2, a_g symmetry). Consequently, the energies of symmetrically allowed ππ* and nπ* states are close, that is crucial for understanding the spectral and photophysical behavior. TD DFT calculations in DMSO show quite clear behavior (Table 2). There is one allowed (A_u symmetry, ππ* type) spectral transition in a visible range for both DPPs, while two transitions of ππ* and nπ* character (both A_u) appear for both DTPPs. The mutual position and intensity of both transitions in DTPPs is sensitive to relatively small geometrical changes through the mixing of both electronic monoexcitations in configurational interaction. Thus increasing a phenyl twist angle in **Ph-DTPP** leads to hypsochromic and hypochromic shift of ππ* transition and opposite bathochromic and hyperchromic shift of nπ* transition. There is a dramatic increase of an intensity of nπ* transition when going from planar *s-cis* to quasiplanar *s-trans* conformer of **Th-DTPP**, so only a minor portion of the latter in solution can cause an observation of this transition in absorption. Thus a long wavelength shoulder in **Ph-DTPP** and **Th-DTPP** spectra in DMSO can be ascribed to a manifestation of nπ* transitions, arising from either phenyl or thiophenyl twists. Furthermore, we suppose, that an absence of fluorescence of both DTPPs in solutions raises from the same reason as proved for thionated peryleneimides, i.e. an efficient competitive ISC of S(nπ*)→T(ππ*) type [18].

There are at least two important reasons for an attempt to understand the nature of solid-state absorption spectra (SSA) of thin layers. First, the absorption edge is crucial for the photovoltaic efficiency, and second, some kinds of nearest-neighbour packing, especially stacking important for transfer processes, can be derived from a shape of the spectrum. The SSA spectra were interpreted using TD DFT calculations of the excitation energies carried out on the model centrosymmetrical dimer geometries, obtained by a reoptimization of a nearest-neighbour (stacked in most cases) geometry, starting from a suitable XRD geometry. In some cases, the dimer optimization did not converge to the required geometry, so the higher oligomers (stacked tetramer, stacked hexamer with three H-bonded molecules in a layer) had to be optimized and final central dimer was extracted from an optimized oligomers. If only one allowed HOMO-LUMO ππ* transition is present in a visible area, as in the case of both DPP centrosymmetrical monomers, it is split into four new ππ* states in a centrosymmetrical dimer (upper and lower Frenkel state (FR) and two charge-transfer states (CT)) [38]. The transition to one of FR and one of CT states (A_u) is always allowed and the other (A_g) is symmetry forbidden. The output of TD DFT calculations produces all these four states adiabatic. For DTPPs the situation is more complicated as both ππ* and nπ* states are split, although nπ* states to a smaller extent, so in summary eight transitions fall into the visible area, four of them being symmetry allowed and theoretically observable in SSA. The aim of the calculations was 1) to characterize the symmetry of the lowest excited state as H/J – aggregates are unambiguously defined by a higher/lower energy of bright (carrying the oscillator strength) excited state with respect to the dark one, irrespective to whether the transition energy of an aggregate bright state lies under or bellow as compared to the monomer [39], 2) to establish the energy difference between the upper and lower FR, relating to a ππ* transition, as one half of it defines excitonic coupling ΔE_{EC} [40] and, consequently, the vibronic pattern of an aggregate (R_{ABS}) [36] and 3) to establish, whether usually weaker transitions to CT and nπ* states, with usually blurred vibronic structure [19,41], may affect the SSA spectra.

The complete results of quantum chemical calculations can be found in ESI. Quite a clear picture was found for both DPPs. **Th-DPP** in both hypothetical modification, taken into account (Fig. 5cd), is an H-aggregate, but ΔE_{EC} is very low for a stack 5c (0.008 eV) and quite high (0.124 eV) for 5d. As R_{ABS} dramatically raises, when going from solution to TL (Fig. 6), the arrangement 5c (very similar to that found for **Th-DTPP** on Fig. 3a)) can be excluded and a stack pattern similar to that one found for β-branched alkyl derivatives of **Th-DPP** seems acceptable, as SSA spectrum of **Th-DPP** is very similar to its 2-ethyl-hexylated derivative [10h]. The allowed CT state with non negligible f_{osc} lies relatively close to the upper FR state (0.20 eV) and contributes to an increase of R_{ABS}. **Ph-DPP** evaporated films are supposed to form the modification similar to P.R. Red 254 (file WEBKET) and the modification same as in single crystal (file SAPDES01) is achieved after solvent vapor annealing [9a,b]. This conclusion relates very well with model calculations. Although both dimers are H-aggregates, ΔE_{EC} is small (0.011 eV) for WEB dimer, leaving R_{ABS} almost unchanged, when going from solution to TL. On the other hand, the dramatic increase of the second and third progression in SSA for vapor annealed TL has two sources for SAP dimer: considerably bigger ΔE_{EC} (0.083 eV) and the dramatic increase of an intensity of the upper CT state, lying 0.27 eV under upper FR state. Theoretical red shift, when going from monomer to the WEBKET-like dimer in vacuum is 0.07 eV, while when going from DMSO maximum to TL maximum, the red shift is 0.16 eV. The difference (0.09 eV) goes on account of so-called crystal shift. The dimer of **Th-DPP** with high ΔE_{EC} shows theoretically slight blue shift (−0.05 eV), as usual for stronger H-aggregates, while the experiment shows a red shift 0.12 eV, giving thus a crystal shift a bit higher (0.17 eV), than for **Ph-DPP**.

An investigation of **Th-DTPP** dimer, obtained from the experimentally found geometry, shows very complex spectrum. The calculations give four allowed (A_u) states with the excitation energies within an interval 0.31 eV and with f_{osc} between 0.074 and 0.227, significantly

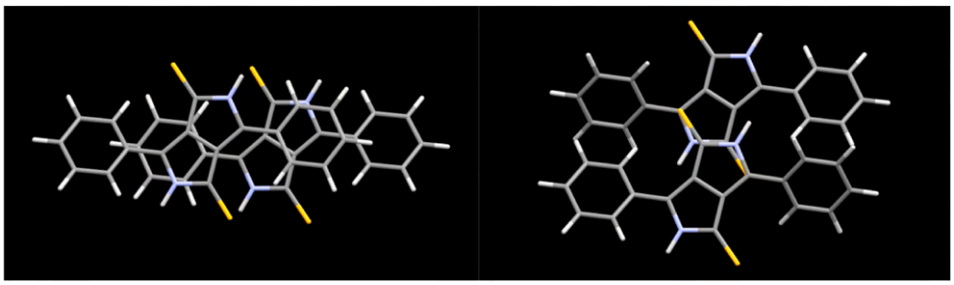

Fig. 8. Model dimers of **Ph-DTPP**, obtained by an reoptimization of SIFLOI01 (left) and SIFLOI02 (right) 3x2 hexamers, followed by an extraction of a central dimer.

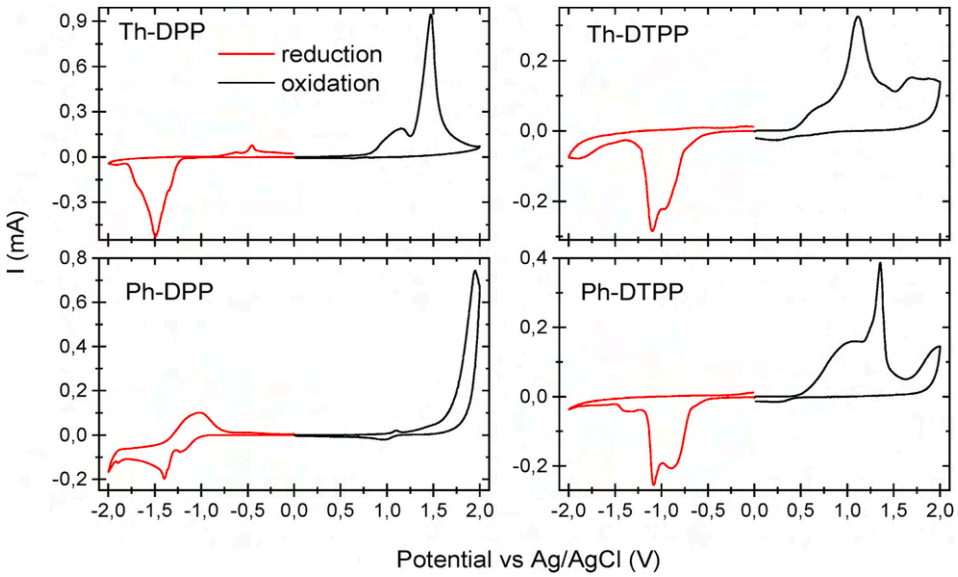

Fig. 9. Voltammograms of measured thin film samples on ITO coated substrates. Measurement was carried out in nitrogen filled glovebox. Used electrolyte was 0.1 M solution of $TBAPF_6$ in anhydrous acetonitrile. Cyclic voltammograms were recorded by scanning potential from 0 to 2.0 or −2.0 V vs Ag/AgCl QRE, with the scanning rate of 25 mV s^{-1}.

broadening the overall spectral band. Two lowest states are formed by lower and upper FR ππ* states with ΔE_{EC} = 0.038 eV, i.e. moderate strength H-aggregate is formed. Nevertheless, its vibronic structure is significantly affected by a close lying (0.10 eV) nπ* state, which is also responsible for a long wavelength tailing. The theoretical monomer-to-dimer red shift is 0.08 eV, while the DMSO-to-TL red shift is 0.13 eV, giving relatively small (0.05 eV) crystal shift. Nevertheless, the position of an experimental spectral maximum in TL can be also affected by a proximity of nπ* transition, as for other spectral features. There were generated four model dimer geometries for **Ph-DTPP**, the two most relevant to experimental SSA spectra are shown on Fig. 8. The former dimer (from SIFLOI01) is stacked, while the latter (from SIFLOI02), with an opposite sense of phenyl twists, is holding together by CH–π attraction between phenyls. The former arrangement forms H-aggregate (S_1 state is A_g), while the latter is J-aggregate (S_1 state is A_u). Consequently, the arrangement, relating to SIFLOI02 modification shows strong solid-state fluorescence in near infrared area [12a], as compared to the weak one for SIFLOI01 modification, observed also in this work (Fig. S13). While the lowest excited state of the former model dimer is always (irrespective on the twist angles) of A_g (ππ*) type, the character of the lowest symmetry allowed A_u state depends strongly on phenyl twists, being ππ* for smaller twists and nπ* for higher twist angles. Consequently, the infrared shoulder in SSA spectrum with varying intensity [12a] is given by a degree of nonplanarity of stacked **Ph-DTPP** molecules in TL, separating and intensifying the long wavelength nπ* transition.

Table 3
E_{HOMO}, E_{LUMO} and E_{gap} obtained by the electrochemical measurements and E_{gap} obtained by optical measurements.

Compound	E_{HOMO} (eV)	E_{LUMO} (eV)	E_{gap} (eV) (CV estimate)	E_{gap} (eV) (optical)
Th-DPP	−6.0	−3.9	2.1	2.0
Th-DTPP	−5.6	−4.5	1.1	1.5
Ph-DPP	−6.2	−4.1	2.1	2.1
Ph-DTPP	−5.7	−4.5	1.2	1.4

3.4. Electrochemistry

To estimate the HOMO and LUMO energy levels of all derivatives, we performed cyclic voltammetry measurements on their evaporated thin film coated on ITO coated glass substrates. All DPPs and DTPPs exhibited both oxidation and reduction peaks within the studied potential window (Fig. 9). However, their re-oxidation and re-reduction currents were substantially low since the oxidized and reduced forms were soluble in the electrolyte, indicating irreversible behavior. E_{HOMO}, E_{LUMO} and bandgap energy (E_{gap}) obtained by electrochemical and optical measurements are summarized in Table 3. Comparing to **Ph-DPP**, **Th-DPP** showed increased E_{HOMO} and E_{LUMO}, however, both have same E_{gap} of 2.1 eV. While optical measurements showed slight decreased E_{gap} found in **Th-DPP**. With the introduction of thioketo groups in DTPP derivatives, increase in E_{HOMO} and decrease in E_{LUMO} were observed, resulting in smaller E_{gap} of 1.1–1.2 eV. While optical E_{gap} were found in

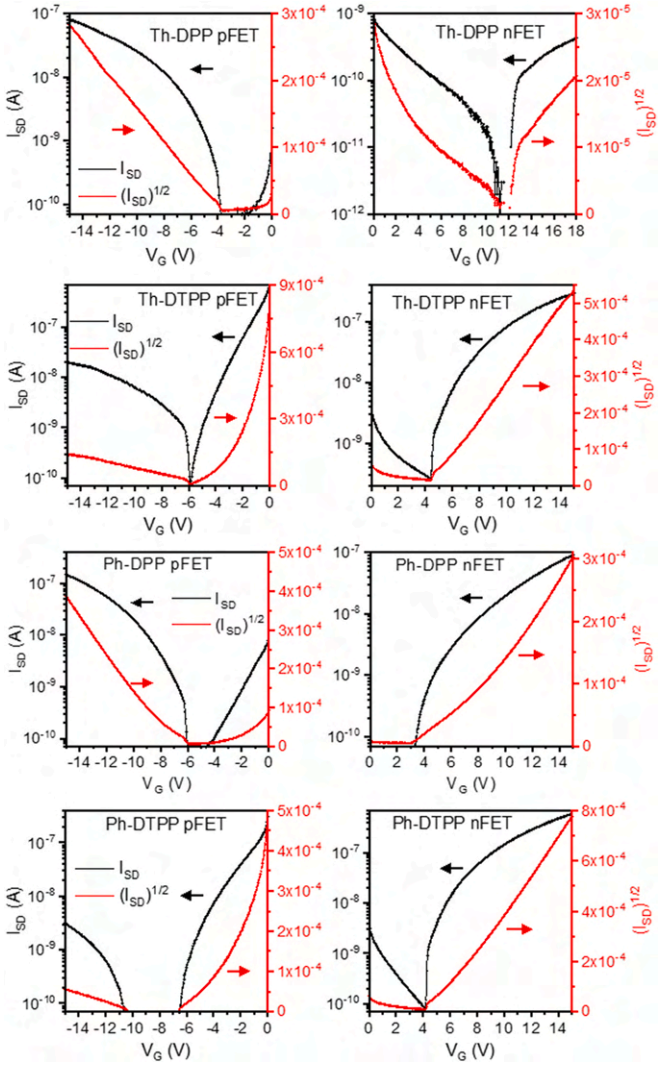

Fig. 10. Transfer characteristics of OFET devices with Au source-drain electrodes (left) and Al source-drain electrodes (right). The measurement parameters were $V_D = (-)15$ V and V_G step of 0,05 V.

the range of 1.4–1.5 eV (Fig. S8). Qualitatively, the theoretically predicted trend (Fig. 7), i.e. the stabilization of LUMO energy, destabilization of HOMO and consequent decrease of a gap upon thionation, was confirmed. Semiquantitatively, the observed LUMO energy stabilization around 0.5 eV upon thionation relates to the theory, while the experimental HOMO destabilization (0.4–0.5 eV) is much higher than predicted (< 0.1 eV). Consequently, considerably low (with respect to the optical one) electrochemical gap of DTPPs goes on account of not very clear decrease of oxidation potential during CV experiment on TL surface. The most probable reason is the interface barrier between the solution and the electrode surface.

3.5. OFET performance

In order to investigate the effect of thionation on charge transport, we have fabricated OFETs with above-mentioned procedures using the four materials as active layer in the device structures. The transfer curves were measured in the probe station placed in a nitrogen-filled glovebox connected to an Agilent B1500A semiconductor parameter analyzer. All transistors based on Al source-drain contacts exhibited typical n-type transport (Fig. 10) with a field-effect electron mobility of 10^{-2}-10^{-3} cm^2/Vs except **Th-DPP** showing quite poor behavior with only a low mobility of about 10^{-5} cm^2/Vs. Additionally, **Th-DPP** revealed a much larger threshold voltage and small current on/off ratio while the other three transistors' are around V_{th} = 3–4 V and on/off ratio = 10^3. On the other hand, both DTPPs present higher electron mobility values. The field-effect hole mobilities in Au source-drain contacts (Fig. 10) were calculated as ≈ 10^{-3} cm^2/Vs for **Th-DPP** and **Ph-DPP** and one order of magnitude lower (≈10^{-4} cm^2/Vs) for both DTPPs. **Th-DPP** in this case shows the best performance, especially, in terms of threshold voltage. All the field-effect mobility values are summarized in Table 4. The values of electron mobilities of **Th-DPP** and **Ph-DPP** around ≈10^{-2} cm^2/Vs are comparable to the values of materials used in OPV [42], although only comparable or lower compared to the values published for DPP-based OFET devices (10^{-2}–10^{-1} cm^2/Vs) [9,10,22,23].

Table 4
Field effect mobilities threshold voltages and on/off values of studied materials of studied materials.

contact material		Th-DPP	Th-DTPP	Ph-DPP	Ph-DTPP
Al ($cm^2 \cdot V^{-1} \cdot s^{-1}$)	μ_e	$1.2 \cdot 10^{-5}$	$7.4 \cdot 10^{-3}$	$2.7 \cdot 10^{-3}$	$1.8 \cdot 10^{-2}$
Au ($cm^2 \cdot V^{-1} \cdot s^{-1}$)	μ_h	$2.0 \cdot 10^{-3}$	$4.9 \cdot 10^{-4}$	$6.6 \cdot 10^{-3}$	$3.0 \cdot 10^{-4}$
Al (V)	V_{th}	12.2	4.4	3.2	4.1
Au (V)	V_{th}	−3.7	−5.9	−6.0	−10.6
Al	on/off	$\sim 10^2$	$\sim 10^3$	$\sim 10^3$	$\sim 10^4$
Au	on/off	$\sim 10^3$	$\sim 10^2$	$\sim 10^3$	$\sim 10^1$

AFM images show that the substituted thiophene derivative (**Th-DTPP**) presents smaller crystallites and rougher surface than the unsubstituted thiophene derivative (**Th-DPP**). On the other hand, the unsubstituted phenyl derivative (**Ph-DPP**) has clear needle-like crystallites, unlike the thionated phenyl derivative (**Ph-DTPP**), which presents more regularly shaped crystallites and slightly smoother surface area (Figs. 11 and 12).

4. Conclusions

In summary, thionation of diketopyrrolopyrrole pigments affects both the molecular structure, and solid-state packing, with the implications to electronic structure, optical and semiconducting properties. Dithioketopyrrolopyrrole pigments remain thermally stable, due to the strong hydrogen bonding. Their molecular structure is more flexible with respect to aryl twists and thus affected by crystal packing. The electronic structure is characterized by low lying LUMO orbital and high lying n-orbital, determining the spectral and photophysical properties. The solid-state absorption edge of DTPPs is shifted to the near infrared area. The fluorescence in solution is quenched, due to the intersystem crossing from high lying nπ* singlet state to triplet manifold. DTPPs form usually red shifted H-aggregates, but a special packing, forming solid-state fluorescent J-aggregate is possible, due to the molecular flexibility. Thionation switches p-type DPP semiconductors to n-type DTPP semiconductors. Altogether, DTPPs can be considered as potential electron accepting components in photovoltaics, due to their NIR absorption, low lying LUMO and n-type mobility.

Author contribution statement

Matous Kratochvil: Conceptualization, Methodology, Validation, Formal analysis, Investigation, Data Curation, Writing - Original Draft, Writing - Review & Editing. *Martin Ciganek*: Conceptualization, Resources, Data Curation, Writing - Original Draft, Writing - Review & Editing, Visualization. *Cigdem Yumusak*: Conceptualization, Methodology, Formal analysis, Writing - Original Draft, Supervision, Project administration. *Hathaichanok Seelajaroen*: Writing - Original Draft, Supervision. *Ivana Cisarova*: Formal analysis, Investigation. *Jan Fabry*: Formal analysis, Investigation, Writing - Original Draft, Writing - Review & Editing. *Martin Vala*: Funding acquisition. *Stanislav Lunak*: Methodology, Software, Formal analysis, Writing - Original Draft, *Martin Weiter*: Supervision, Funding acquisition. *Niyazi Serdar Sariciftci*:

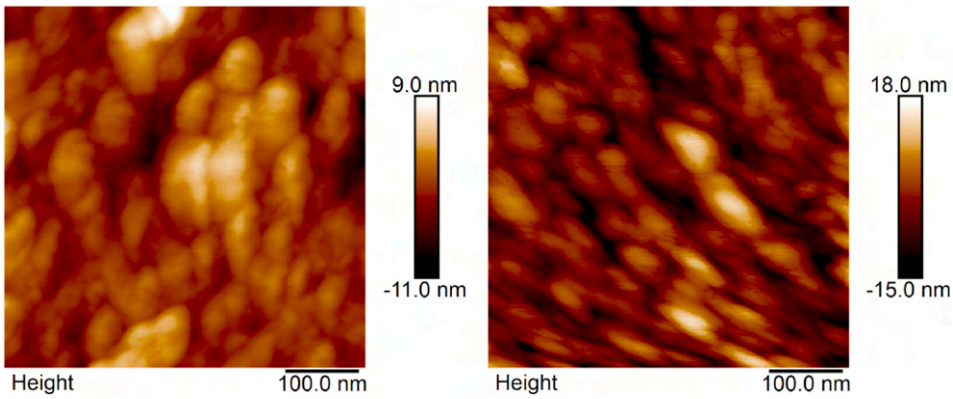

Fig. 11. Topography of thin films of **Th-DPP** (left) and **Th-DTPP** (right).

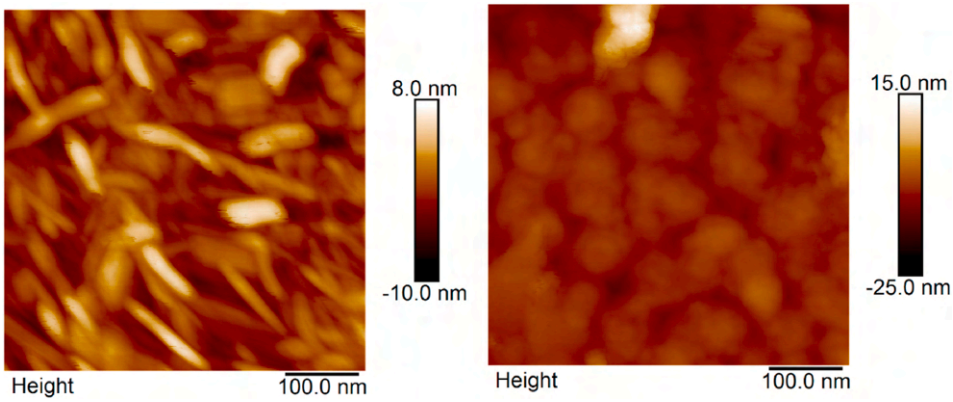

Fig. 12. Topography of thin films of **Ph-DPP** (left) and **Ph-DTPP** (right).

Supervision, Project administration, Funding acquisition. *Jozef Krajcovic*: Conceptualization, Data Curation, Supervision, Project administration, Funding acquisition.

Declaration of competing interest

The authors declare that they have no known competing financial interests or personal relationships that could have appeared to influence the work reported in this paper.

Acknowledgements

The authors thank for their financial support the Ministry of Industry and Trade TRIO (project No. FV20022), the Czech Science Foundation grant No. 19-22783S and Austrian Agency for International Cooperation in Education and Research (OEAD-GmbH, WTZ, CZ01/2020, 8J20AT025). Access to computing and storage facilities owned by parties and projects contributing to the National Grid Infrastructure MetaCentrum provided under the programme "Projects of Large Research, Development, and Innovations Infrastructures" (CESNET LM2015042) is greatly appreciated by S.L. M.K. gratefully acknowledges financial support within BUT project FCH-S-21-7553.

Appendix A. Supplementary data

Supplementary data to this article can be found online at https://doi.org/10.1016/j.dyepig.2021.109884.

References

[1] Zhou R, Jiang Z, Yang Ch, Yu J, Feng J, Adil MA, Deng D, Zou W, Zhang J, Lu K, Ma W, Gao F, Wei Z. Nat Commun 2019;10:5393.
[2] Cheng P, Li G, Zhan X, Yang Y. Nat Photonics 2018;12:131–42.
[3] a) Dhar J, Salzner U, Patil S. J Mater Chem C 2017;5:7404–30.b) Quinn JTE, Zhu J, Li X, Wang J, Li Y. J Mater Chem C 2017;5:8654–81.c) Okamoto T, Kumagai S, Fukuzaki E, Ishii H, Watanabe G, Niitsu N, Annaka T, Yamagishi M, Tani Y, Sugiura H, Watanabe T, Watanabe S, Takeya J. Sci. Adv. 2020;6:aaz0632.
[4] Usta H, Risko C, Wang Z, Deliomeroglu H, Zhukhovitskiy MK, Facchetti A, Marks TJ. J Am Chem Soc 2009;131:5586–608.
[5] Irimia-Vladu M, Kanbur Y, Camaioni F, Coppola ME, Yumusak C, Irimia CV, Vlad A, Operamolla A, Farinola GM, Suranna GP, González-Benitez N, Molina MC, Bautista LF, Langhals H, Stadlober B, Glowacki ED, Sariciftci NS. Chem Mater 2019;31:6315–46.
[6] Venkateswararao A, Wong KT. Bull Chem Soc Jpn 2021;94:812–38.
[7] a) Iqbal A, Jost M, Kirchmayr R, Pfenninger J, Rochat A, Wallquist O. Bull Soc Chim Belg 1988;97:615–44.b) Hao Z, Iqbal A. Chem Soc Rev 1997;26:203–13.c) Wallquist O. In: Smith HM, editor. In high performance pigments. Wiley-VCH; 2002.
[8] Luňák Jr S, Vyňuchal J, Horáčková P, Frumarová B, Žák Z, Kučeřík J, Salyk O. J Mol Struct 2010;983:39–47.
[9] a) Mizuguchi J, Rihs G. Ber. Bunsenges. Phys. Chem. 1992;96:597–606.b) Mizuguchi J. J Phys Chem A 2000;104:1817–21.c) Glowacki ED, Coskun H, Blood-Forsythe MA, Monkowius U, Leonat L, Grzybowski M, Gryko D, White MS, Aspuru-Guzik A, Sariciftci NS. Org Electron 2014;15:3521–8.
[10] a) Naik MA, Venkatramaiah N, Kanimozhi C, Patil S. J Phys Chem C 2012;116:26128–37.b) Liu J, Zhang Y, Phan H, Sharenko A, Moonsin P, Walker B, Promarak V, Nguyen TQ. Adv Mater 2013;25:3645–50.c) Liu J, Walker B, Tamayo A, Zhang Y, Nguyen TQ. Adv Funct Mater 2013;23:47–56.d) Calvo-Castro J, Maczka S, Thomson C, Morris G, Kennedy AR, McHugh CJ. Cryst Eng Comm 2016;18:9382–90.e) Pop F, Lewis W, Amabilino DB. Cryst Eng Comm 2016;18:8933–43.f) Mauck CM, Hartnett PE, Margulies EA, Ma L, Miller CE, Schatz GC, Marks TJ, Wasielewski MR. J Am Chem Soc 2016;138:11749–61.g) Fu C, Bélanger-Gariépy F, Perepichka DF. Cryst Eng Comm 2016;18:4285–9.h) Hartnett PE, Margulies EA, Mauck CM, Miller CE, Wu Y, Wu YL, Marks TJ, Wasielewski MR. J Phys Chem B 2016;120:1357–66.i) Stolte M, Suraru SL, Diemer P, Hao T, Burschka Ch, Zschieschang U, Klauk H, Würthner F. Adv Funct Mater 2016;26:7415–22.j) Kovalenko A, Yumusak C, Heinrichová P, Střítský S, Fekete L, Vala M, Weiter M, Sariciftci NS, Krajčovič J. J Mater Chem C 2017;5:

4716–23.k) Genevaz N, Chávez P, Untilova V, Boeglin A, Bailly C, Karmazin L, Biniek L. J Mater Chem C 2018;6:9140–51.l) Saes BWH, Lutz M, Wienk MM, Meskers SCJ, Janssen RAJ. J Phys Chem C 2020;124:25229–38.m) Rais D, Toman P, Pfleger J, Acharya U, Panthi YR, Menšík M, Zhigunov A, Thottappali MA, Vala M, Marková A, Stříteský S, Weiter M, Cigánek M, Krajčovič J, Pauk K, Imramovský A, Zaykov A, Michl J. ChemPlusChem 2020;85:2689–703.

[11] a) Closs F, Gompper R. Angew Chem Int Ed 1987;26:552–4.b) Grzybowski M, Gryko DT. Adv. Opt. Mater. 2015;3:280–320.

[12] a) Mizuguchi J, Rochat AC, Rihs G. Ber. Bunsenges. Phys. Chem. 1992;96:607–18. b) Mizuguchi J. J Phys Chem A 2001;105:1125–30.

[13] Lévesque S, Gendron D, Bérubé N, Grenier F, Leclerc M, Côté M. J Phys Chem C 2014;118:3953–9.

[14] a) Qian G, Qi J, Davey JA, Wright JS, Wang ZY. ChemMater 2012;24:2364–72.b) Qian G, Wang ZY. Adv Mater 2012;24:1582–8.c) Qian G, Qi J, Wang ZY. J Mater Chem 2012;22:12867–73.

[15] Ripaud E, Demeter D, Rousseau T, Boucard-Cétol E, Allain M, Po R, Leriche P, Roncali J. Dyes Pigments 2012;95:126–33.

[16] Welterlich I, Tieke B. Polym Chem 2013;4:3755–64.

[17] a) Gendron D, Maasoumi F, Armin A, Pattison K, Burn PL, Meredith P, Namdas EB, Powell BJ. RSC Adv 2017;7:10316–22.b) Zhang H, Yang K, Zhang K, Zhang Z, Sun Q, Yang W. Polym Chem 2018;9:1807–14.

[18] Tilley AJ, Pensack RD, Lee TS, Djukic B, Scholes GD, Seferos DS. J Phys Chem C 2017;118:9996–10004.

[19] Luňák Jr S, Nepraš M, Kurfürst A, Kuthan J. Chem Phys 1993;170:67–76.b) Luňák Jr S, Nepraš M, Hrdina R, Kurfürst A, Kuthan J. Chem Phys 1993;170:77–80.

[20] El Sayed MA. J Chem Phys 1963;38:2834–8.

[21] Suraru SL, Zschieschang U, Klauk H, Würthner F. Chem Commun 2011;47:1767–9.

[22] Ruiz-Carretero A, Rovelo NRA, Militzer S, Mésini PJ. J Mater Chem A 2019;7:23451–75.

[23] Zhang H, Deng R, Wang J, Li X, Chen YM, Liu K, Taubert CJ, Cheng SZD, Zhu Y. ACS Appl Mater Interfaces 2017;9:21891–9.

[24] Zhang H, Liu M, Yang W, Judin L, Hukka TI, Priimagi A, Deng Z, Vivo P. Adv. Mater. Interfaces 2019;6:1901036.

[25] a) Luňák Jr S, Havel L, Vyňuchal J, Horáková P, Kučerík J, Weiter M, Hrdina R. Dyes Pigments 2010;85:27–36.b) Cigánek M, Heinrichová P, Kovalenko A, Kučerík J, Vala M, Weiter M, Krajčovič J. Dyes Pigments 2020;175:108141.

[26] Mardare AI, Kaltenbrunner M, Sariciftci NS, Bauer S, Hassel AW. Phys Status Solidi 2012;209:813–8.

[27] Głowacki ED, Coskun H, Blood-Forsythe MA, Monkowius U, Leonat L, Grzybowski M, Gryko D, White MS, Aspuru-Guzik A, Sariciftci NS. Org Electron 2014;15:3521–8.

[28] Smith TJ, Stevenson KJ. In Handbook of electrochemistry. Amsterdam: Elsevier; 2007. p. 73–110.

[29] Cardona CM, Li W, Kaifer AE, Stockdale D, Bazan GC. Adv Mater 2011;23:2367–71.

[30] Palatinus L, Chapuis G. J Appl Crystallogr 2007;40:786–90.

[31] Petříček V, Dušek M, Palatinus L. Z für Kristallogr - Cryst Mater 2014;229:345–52.

[32] Spek AL. Acta Crystallogr Sect D Biol Crystallogr 2009;65:148–55.

[33] Gaussian 09, Revision D.01, Frisch MJ, Trucks WG, Schlegel HB, Scuseria GE, Robb MA, Cheeseman JR, Scalmani G, Barone V, Mennucci BG, Petersson A, Nakatsuji H, Caricato M, Li X, Hratchian HP, Izmaylov AF, Bloino J, Zheng G, Sonnenberg JL, Hada M, Ehara M, Toyota K, Fukuda R, Hasegawa J, Ishida M, Nakajima T, Honda Y, Kitao O, Nakai H, Vreven T, Montgomery Jr JA, Peralta JE, Ogliaro F, Bearpark M, Heyd JJ, Brothers E, Kudin KN, Staroverov VN, Kobayashi R, Normand J, Raghavachari K, Rendell A, Burant JC, Iyengar SS, Tomasi J, Cossi M, Rega N, Millam JM, Klene M, Knox JE, Cross JB, Bakken V, Adamo C, Jaramillo J, Gomperts R, Stratmann RE, Yazyev O, Austin AJ, Cammi R, Pomelli C, Ochterski JW, Martin RL, Morokuma K, Zakrzewski VG, Voth GA, Salvador P, Dannenberg JJ, Dapprich S, Daniels AD, Farkas Ö, Foresman JB, Ortiz JV, Cioslowski J, Fox DJ, Wallingford CT. Gaussian. Inc.; 2009.

[34] a) Mizuguchi J, Rochat AC, Rihs G. Acta crystallogr., C Cryst. struct. commun. 1990;46:1899–903.b) Groom CR, Bruno IJ, Lightfoot MP, Ward SC. Acta Crystallogr B: Struct. Sci., Cryst. Eng. Mater. 2016;72:171–9 (version 5.41 from November 2019 with updates up to May 2020).c) Mizuguchi J, Arita M, Rihs G. Acta crystallogr., C Cryst. struct. commun. 1991;47:1952–6.

[35] Macrae CF, Sovago I, Cottrell SJ, Galek PTA, McCabe P, Pidcock E, Platings M, Shields GP, Stevens JS, Towler M, Wood PA. J Appl Crystallogr 2020;53:226–35.

[36] Hestand NJ, Spano FC. Chem Rev 2018;118:7069–163.

[37] Planar centrosymmetrical geometries form the minima for both s-cis and s-trans arrangements of Th-DPP and s-cis conformation of Th-DTPP. For s-trans arrangement of Th-DTPP almost planar Ci geometry, used in Fig. 7, gives one imaginary frequency (i14 cm-1) and the only minimum is found at C2 symmetry with twist angles about 172°, i.e. closer to experiment, but with wrong symmetry of a monomer. The highest difference between the orbital energies for both Ci and C2 symmetries of s-trans Th-DTPP is about 0.003 eV. If optimized on ωB97X-D/6-311G(d,p) level, the situation is different: s-trans Th-DTPP Ci minimum is twisted (169°) and without imaginary frequencies, while in s-cis arrangement optimization under both Ci and C2 symmetry gives almost planar structures with i10 cm-1 and i4 cm-1, respectively, i.e. optimized monomer structure is unsymmetrical contrary to the experiment.

[38] Bellinger D, Pflaum J, Brüning C, Engel V, Engels B. Phys Chem Chem Phys 2017;198:2434–48.

[39] Zheng C, Zhong C, Collison CJ, Spano FC. J Phys Chem C 2019;123:3203–15.

[40] Shi J, Suarez LEA, Yoon SJ, Varghese S, Serpa C, Park SY, Lüer L, Roca-Sanjuán D, Milián-Medina B, Gierschner J. J Phys Chem C 2017;121:23166–23183K.

[41] Luňák Jr S, Nepraš M, Hrdina R, Mustroph H. Chem Phys 1994;184:255–60.

[42] Li Y, Gu M, Pan Z, Zhang B, Yang X, Gu J, Chen Y. J Mater Chem 2017;5:10798–814.